LA-UR-21-28905
Approved for public release; distribution is unlimited.

Title: Closures and Simulation for Thermal Radiation Transport in Stochastic Media with Nonlinear Temperature Dependence

Author(s): Skinner, Corey Michael

Intended for: Report

Issued: 2021-09-28 (rev.1)

Closures and Simulation for Thermal Radiation Transport in Stochastic Media with Nonlinear Temperature Dependence

Research Proposal for Doctoral Dissertation

University of New Mexico

Corey Skinner

Advised by Anil Prinja

1. Introduction

Applications frequently arise in which it is not feasible to produce an accurate solution to the transport equation due to highly heterogeneous spatial (and temporal) variations in the physical properties of the medium. Examples include: inertial confinement fusion (ICF), where Rayleigh-Taylor instabilities lead to spatially complex structures composed of chunks of solid material randomly dispersed in background plasma [1]; representing clouds in atmospheric radiative transfer models [2]; the so-called double-heterogeneity problem in pebble-bed nuclear reactors that comprises a random configuration of fuel-moderator pebbles, each containing fuel pellets randomly dispersed in a graphite matrix [3]; multiphase effects in boiling water reactors as well as potentially in liquid-fuel reactors and molten salt reactors.

Because of the practical challenge of rendering very complex realistic spatial structures for numerical work, it is common practice to resort to characterizing such media as stochastic mixtures of materials, ideally parametrized with low order statistics such as the mean, variance, and correlation functions of the now random material properties. This enables realizations of the medium to be repeatedly generated and radiation transport computations to, in principle, be performed for a large ensemble of these realizations to obtain a statistically well-characterized radiation field. Statistical post-processing yields desired quantities such as conditional and unconditional mean radiation flux and probability distributions of transmitted radiation. However, such computations prove expensive for all but the simplest stochastic geometries and are most suited for benchmarking approximate models. The most common approximations lead to homogenized media so that transport computations are required only on a single medium realization but by construct provide only limited statistical information on the radiation field. Almost all approximate approaches to this problem attempt to develop equations for low order moments of the radiation intensity (mean, second moment, correlation function) but inevitably encounter a closure problem: the equation for any statistical moment will contain terms depending on unknown higher-order moments. Thus, the challenge shifts to one of developing closure relations that relate the unknown moments to the lower-order moments. Under very special conditions, an exact closure can be derived but in general closures are heuristically stated constitutive relations. Also, closure approaches depend on whether the mixing statistics are spatially and/or temporally continuous as in fluctuating turbulent fields, or discontinuous as in randomly mixed solid chunks of material. Thus, unconditional averaging is generally applied in the former case but

conditional averaging is more appropriate when the mixing is discontinuous. In this work, the emphasis is on binary statistical mixtures of immiscible fluids as as such the quantities of interest are averages (flux, temperature) conditioned on the material type.

The simples homogenized medium approximation is the atomic mix approximation where the random cross-sections (equivalently opacities in the context of thermal radiation transport) are replaced by deterministic material volume fraction weighted averages [4]. However, this approximation is valid only when the particle mean free path is much longer than the mean chord length of each material so that on average the particle samples many material changes before colliding. The volume fraction is then the only statistical parameter required to characterize the mixture. Although only a single transport solve is required in the atomic mix approximation, the solution is valid only under conditions of weak stochastic effects.

More realistic modeling requires development of higher-order homogenized material models which more accurately describe strong mixing when the statistics are known. One such situation that has become a paradigm in this field is Markovian mixing wherein the individual material chunk thicknesses are exponentially distributed [1]. When additionally both materials are nonscattering or nonemitting, i.e., there is no angular redistribution of the radiation, the stochastic process representing material mixing and transport is jointly Markovian and an exact pair of coupled equations can be written down for the averaged flux conditioned on the material type [1]. However, when one or both materials are also scattering or reemitting, the resulting angular redistribution of radiation makes the joint process non-Markovian and a closure is required to obtain a similar pair of equations for the material averaged fluxes. In the absence of an exact closure, heuristic closures have been developed leading to an inexact model. The best knokwn and widely employed is the so-called Levermore-Pomraning (LP) closure which amounts to making a Markovian assumption and hence has the advantage of becoming exact in the absence of angular redistribution [5]. The model error depends on the extent of scattering and overall medium thickness and can be significant when the medium is diffusive. Nevertheless, the LP model is robust and easily implemented, requiring the solution of only two transport equations (essentially a two-group model) and therefore does not require much additional computational effort beyond the atomic mix model while yielding greater accuracy.

The closure method was originally developed for the radiation field only but was subsequently extended to apply to thermal radiation transport in participating media where the material temperature is an additional unknown stochastic variable [6]. However, the

dependence of physical properties (opacity, density, specific heat) on temperature makes the coupled problem nonlinear and further weakens the validity of the LP closure. Investigations have therefore been restricted to the linear version of the coupled problem for which the original conditions for the application of the LP closure are restored. To date, a systematic extension of the stochastic approach to account for nonlinear temperature dependence has not been developed, although heuristic generalizations have been attempted. Moreover, most of the work on stochastic thermal radiation transport has been restricted to 1D planar geometry with Markovian mixing where medium realizations are easily generated. Implementation in higher dimensions have not been attempted but interesting applications to multidimensional stochastic geometries in the neutron transport context have been recently presented [7].

In this dissertation, two generalizations of work to date on thermal radiation transport in participating stochastic media are proposed. In the first, an approach is presented that accounts for nonlinearities without approximation in the stochastic formulation. Numerical tests are carried out for a special problem where material transitions occur in time only. This ensures the closure is exact and enables a systematic numerical evaluation of the effects of dependence of physical properties on the random temperature by comparing against heuristic models. In the second, 1D and 2D stochastic geometries will be implemented in the LANL Branson Implicit Monte Carlo (IMC) coupled thermal radiation - material temperature code. The goal here is a detailed numerical investigation of the accuracy of the LP closure, known as the chord length sampling (CLS) algorithm, in 1D and 2D in a realistic setting, with 2D random geometries generated based on the Box-Poisson algorithm recently implemented for nuclear criticality applications [7]. Specific problems to be investigated include (i) exploring an earlier hypothesis that the LP closure is more accurate in 2D than in 1D due to reduced correlation, and (ii) assessing if the previously demonstrated result in the radiation-only case that the diffusion limit for 1D planar random media is the atomic mix diffusion equation extends to the coupled case and if it also holds in 2D. Finally, time permitting, a heuristic non-Markovian extension of the LP closure will be considered that allows for memory effects near material interfaces.

2. Transport in Binary Statistical Media

Frequently in studies of stochastic media, the media in question is represented as a binary system of immiscible, non-participating materials structured according to discontinuous mixing statistics [8]. An example illustration of a binary stochastic media which could result from an inertial confinement fusion experiment subjected to a thermal radiation fluence is seen in Figure 1. In this image, note that the phrasing "optically thin" simply refers to a smaller relative value of material opacity, while "optically thick" refers to the larger value thereof.

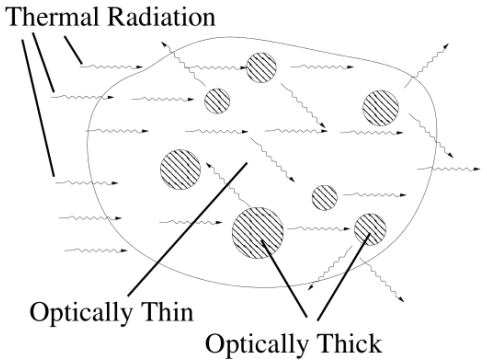

Figure 1: Thermal Radiation Propagating in Binary Stochastic Media

These materials within the system are characterized by a statistical representation of relevant properties of the spatial geometry. Typically, such a characterization involves the use of a mean chord length, λ_i, within material i, defined such that if a ray extending an infinite distance were cast through any arbitrary direction in the material, the average distance comprised of each material between transitions would by the law of large numbers approach the mean chord length. This parameter is directly related to the volume fraction p_i of each material, as seen in equations (1) and (2):

$$p_1 = \frac{\lambda_1}{\lambda_1 + \lambda_2} \tag{1}$$

$$p_2 = \frac{\lambda_2}{\lambda_1 + \lambda_2} = 1 - p_1 \tag{2}$$

A Markovian transition of materials is one in which the system statistics do not possess memory of any state preceding its current state, characterized by an exponential distribution parameterized by the mean chord length. Given Poisson statistics for the system, at any given point in space, the probability P that a distance d_i of material i

will be present per unit distance is given by the probability distribution function shown in equation (3):

$$P(i) = \frac{1}{\lambda_i} e^{-\frac{d_i}{\lambda_i}} \tag{3}$$

Equation (3) may be integrated to obtain the cumulative distribution function, and with further algebraic operations an expression for d_i in terms of a random number ξ sampled from a uniform distribution may be obtained, shown in equation (4):

$$d_i = -\lambda_i \ln(\xi) \tag{4}$$

Given specific values for λ_1 and λ_2, a realization of geometry may be generated easily for a one-dimensional case. Such visualizations are shown in Figures 2 and 3. These realizations may be consistent in time, that is, solved within a steady-state model context if geometric stochasticity is the only driving factor of the model, but temporally-varying stochastic models are also viable.

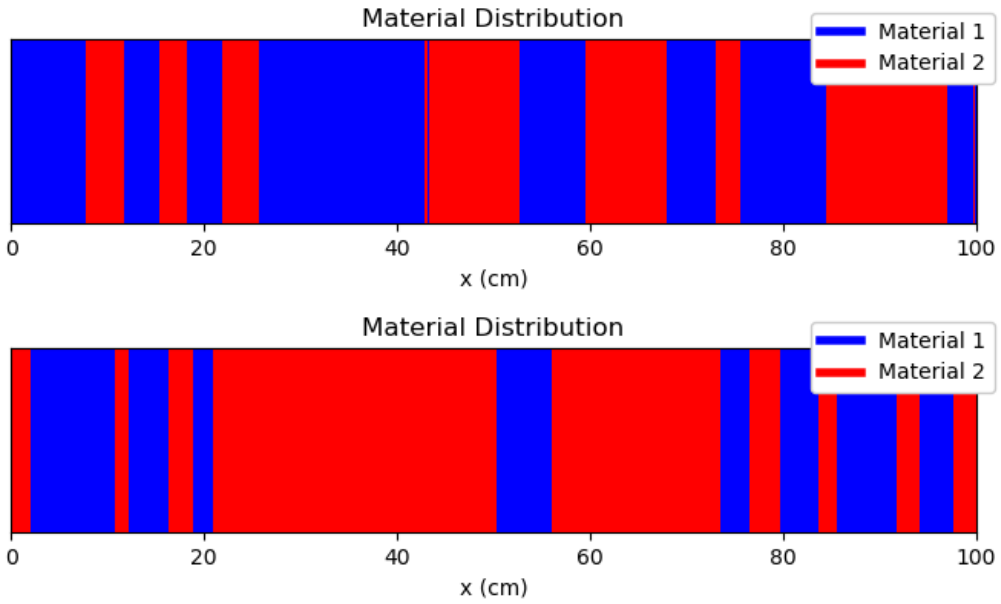

Figure 2: Independent 1D Realizations of $\lambda_1 = \frac{101}{20}$ cm, $\lambda_2 = \frac{101}{20}$ cm

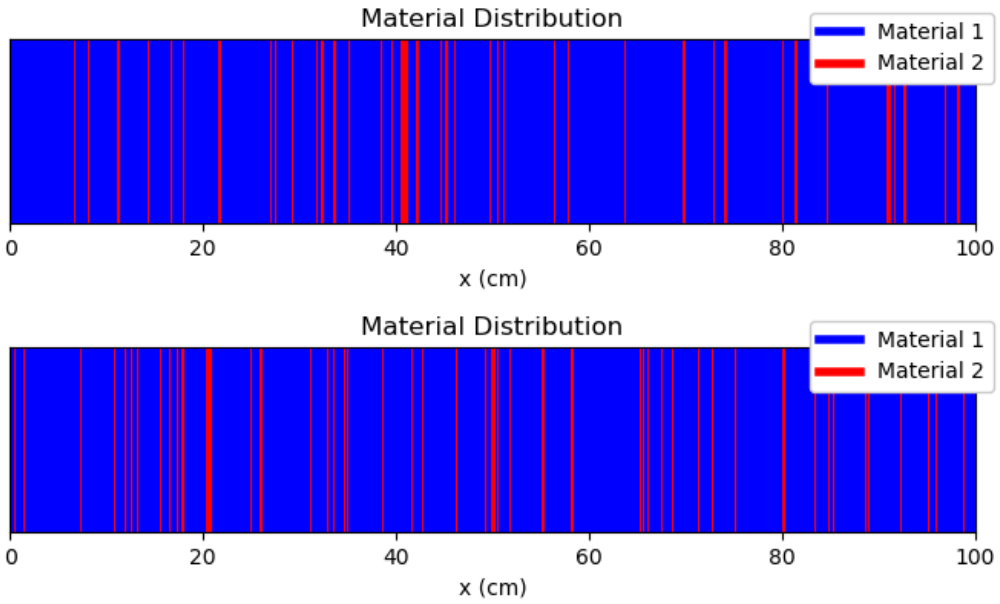

Figure 3: Independent 1D Realizations of $\lambda_1 = \frac{99}{100}$ cm, $\lambda_2 = \frac{11}{100}$ cm

In these figures, the relation between the mean geometric chord length of each material to that material's volume fraction can be seen. Similar mean chord lengths produce similar volume fractions, though subjected to stochastic sampling, while diverse mean chord lengths result in diverse volume fractions, reflective of whichever material is the dominant material in the resulting profiles.

3. Linear Transport

A linear neutral-particle transport equation for a monoenergetic system [5] can be written as seen in equation (5):

$$\frac{1}{v}\frac{\partial\psi\left(\vec{r},\vec{\Omega},t;\omega\right)}{\partial t}+\vec{\Omega}\cdot\vec{\nabla}\psi\left(\vec{r},\vec{\Omega},t;\omega\right)+\sigma_t\left(\vec{r},t;\omega\right)\psi\left(\vec{r},\vec{\Omega},t;\omega\right) = \frac{\sigma_s\left(\vec{r},t;\omega\right)}{4\pi}\int_{4\pi}d\vec{\Omega}'\psi\left(\vec{r},\vec{\Omega}',t;\omega\right)+S\left(\vec{r},\vec{\Omega},t;\omega\right) \quad (5)$$

In this representation, v is the particle velocity, $\vec{\Omega}$ is the particle direction vector, $\vec{r}$ is the spatial location vector, and t is a time value. Material properties of the system are contained in σ_t, the total material cross-section, and σ_s, the material scattering cross-section. $S\left(\vec{r},\vec{\Omega},t;\omega\right)$ is a generic angular particle source term. ψ is the angular flux of the system, defined via a distribution function $f\left(\vec{r},\vec{\Omega},t;\omega\right)$ where $fd\vec{r}d\vec{\Omega}$ describes the number of particles in $d\vec{r}d\vec{\Omega}$ at time t. The relationship between ψ and f is shown in the below equation:

$$\psi\left(\vec{r},\vec{\Omega},t;\omega\right)=vf\left(\vec{r},\vec{\Omega},t;\omega\right) \quad (6)$$

All parameters within equation (5) exist within the context of a single realization of materials governed by known sampling statistics, denoted by ω. Therefore, the linear transport equation may be solved on any one realization of stochastic media, and again on subsequent realizations derived from the same sampling statistics. The ensemble average result of parameters of interest (typically the flux ψ is one such parameter) may be used to approximate low-order moments such as the mean through many such realizations.

3a. Atomic Mix

Deriving a transport equation as (5) for a stochastic media system without the requirement of solving the equation on individual realizations can be done [5]. The simplest approach is to make an atomic mix assumption, which relies on the presupposition that the mean chord length of each material is small relative to the mean free path of the transport particle in question, allowing for a given particle in the system to experience many material transitions before suffering a collision.

The atomic mix model makes the assumption that the solution of the transport equation in a disparate stochastic media is similar to the same equation solved over a homogenized, or atomically mixed, combination of the materials involved. This is accomplished by deriving average quantities of material properties, such as the opacity $\langle \sigma_a (\vec{r}, t) \rangle$, from a sum weighted by the constituent volume fractions of the individual materials. This can be seen in equation (7):

$$\langle \sigma_a (\vec{r}, t) \rangle = p_1 \sigma_{a1} (\vec{r}, t) + p_2 \sigma_{a2} (\vec{r}, t) \tag{7}$$

Other material properties are the specific heat and density, which are similarly weighted by a volume fraction for each material and averaged using a simple sum. The resulting transport equation contains the atomically-mixed material parameters, shown in equation (8):

$$\frac{1}{v} \frac{\partial \left\langle \psi \left(\vec{r}, \vec{\Omega}, t \right) \right\rangle}{\partial t} + \vec{\Omega} \cdot \vec{\nabla} \left(\left\langle \psi \left(\vec{r}, \vec{\Omega}, t \right) \right\rangle \right) + \langle \sigma_t (\vec{r}, t) \rangle \left\langle \psi \left(\vec{r}, \vec{\Omega}, t \right) \right\rangle = \frac{\langle \sigma_s (\vec{r}, t) \rangle}{4\pi} \langle \phi (\vec{r}, t) \rangle + \left\langle S \left(\vec{r}, \vec{\Omega}, t \right) \right\rangle \tag{8}$$

The atomic mix model effectively removes any available streaming paths through whichever material may be the most optically thin from the perspective of a transport particle. This effectively over-approximates the attenuating characteristics of the optically thicker media, regardless of the volume fractions involved in the problem.

The atomic mix model does however exhibit the expected behavior of increasing accuracy as the material chord lengths in the system decrease towards an atomically mixed length. That is, as the material mean chord lengths approach zero relative to the mean free path of the particle, the atomic mix model becomes a more appropriate model to apply.

3b. Levermore-Pomraning Model

A generally more accurate method of approximating the linear transport equation within a stochastic media context involves using ensemble average statistics on each term of the linear transport equation [5]. This process relies on a characteristic function to facilitate the statistical derivation, shown in equation (9):

$$\chi_i\left(\vec{r},t\right)=\begin{cases}0, & \text{if position } \vec{r} \text{ is in material } i \text{ at time } t\\ 1, & \text{otherwise}\end{cases} \tag{9}$$

The ensemble average process results in a conditional system of equations constructed from particle balance properties that are exactly closed in most terms, with the exception of the radiation streaming term due to mixing statistics. The resulting equation from an ensemble average process is shown in the coupled equations (10) and (11), governed by the material definition of equation (12):

$$\begin{aligned}&\frac{1}{v}\frac{\partial p_i\psi_i\left(\vec{r},\vec{\Omega},t\right)}{\partial t}+\vec{\Omega}\cdot\vec{\nabla}\left(p_i\psi_i\left(\vec{r},\vec{\Omega},t\right)\right)+\sigma_{ti}\left(\vec{r},t\right)p_i\psi_i\left(\vec{r},\vec{\Omega},t\right)\\&=\frac{\sigma_{si}\left(\vec{r},t\right)}{4\pi}p_i\int_{4\pi}d\vec{\Omega}'\psi_i\left(\vec{r},\vec{\Omega}',t\right)+p_iS_i\left(\vec{r},\vec{\Omega},t\right)+\frac{p_j\overline{\psi}_j\left(\vec{r},\vec{\Omega},t\right)}{\lambda_j}-\frac{p_i\overline{\psi}_i\left(\vec{r},\vec{\Omega},t\right)}{\lambda_i}\end{aligned} \tag{10}$$

$$\begin{aligned}&\frac{1}{v}\frac{\partial p_j\psi_j\left(\vec{r},\vec{\Omega},t\right)}{\partial t}+\vec{\Omega}\cdot\vec{\nabla}\left(p_j\psi_j\left(\vec{r},\vec{\Omega},t\right)\right)+\sigma_{tj}\left(\vec{r},t\right)p_j\psi_j\left(\vec{r},\vec{\Omega},t\right)\\&=\frac{\sigma_{sj}\left(\vec{r},t\right)}{4\pi}p_j\int_{4\pi}d\vec{\Omega}'\psi_j\left(\vec{r},\vec{\Omega}',t\right)+p_jS_j\left(\vec{r},\vec{\Omega},t\right)+\frac{p_i\overline{\psi}_i\left(\vec{r},\vec{\Omega},t\right)}{\lambda_i}-\frac{p_j\overline{\psi}_j\left(\vec{r},\vec{\Omega},t\right)}{\lambda_j}\end{aligned} \tag{11}$$

$$i,j=1,2 \qquad i\neq j \tag{12}$$

In the above equation, v is the particle velocity. Conditional quantities for materials i and j, conditioned on the material at that location in phase-space being either material i or j, include the conditional angular flux ψ_i and ψ_j, the total cross-section σ_{ti} and σ_{tj}, the scattering cross-section σ_{si} and σ_{sj}, and a distributed source S_i and S_j.

One parameter of interest in solving this equation is the conditional angular flux ψ_i in material i. Solving for this term depends on knowledge of $\overline{\psi}_i$, which is defined as the ensemble average conditional angular flux at internal transition boundaries within the problem domain. It is not trivial to write $\overline{\psi}_i$ in terms of ψ_i, as this is where the closure problem arises. The values for $\overline{\psi}_i$ and $\overline{\psi}_j$ cannot be established *a priori* to computation.

For a time-independent, purely absorbing medium subject to Markovian mixing statistics, it is an exact solution to replace $\overline{\psi}_i$ with ψ_i and $\overline{\psi}_j$ with ψ_j. Such a substitution comprises the Levermore-Pomraning closure model. However, because an exact general formula for $\overline{\psi}_i$ in terms of ψ_i has not been found, the LP closure is of limited utility

when predicting the solution of stochastic media problems. In the event of angular redistribution of any kind, the Markovian closure relationship described by the LP model breaks down.

As stated, the Levermore-Pomraning closure heuristically invokes the use of probabilistic streaming terms [9] by making the substitution seen in equation (13):

$$\overline{\psi}_i\left(\vec{r},\vec{\Omega},t\right)=\psi_i\left(\vec{r},\vec{\Omega},t\right)\qquad\overline{\psi}_j\left(\vec{r},\vec{\Omega},t\right)=\psi_j\left(\vec{r},\vec{\Omega},t\right)\tag{13}$$

The above substitution is a generally heuristic statement that the ensemble average conditional angular flux across material interfaces in the solution domain is equivalent to the volumetrically-averaged conditional angular flux in that location in phase space. This is an accurate statement only in the case of strictly Markovian mixing statistics for the stochastic geometry, and a lack of angular redistribution in the problem either through particle scattering or absorption and subsequent re-emission. The LP closure results in the coupled transport equations seen in equation (14) and (15), similarly governed by the material definition equation (16):

$$\begin{aligned}&\frac{1}{v}\frac{\partial p_i\psi_i\left(\vec{r},\vec{\Omega},t\right)}{\partial t}+\vec{\Omega}\cdot\vec{\nabla}\left(p_i\psi_i\left(\vec{r},\vec{\Omega},t\right)\right)+\sigma_{ti}\left(\vec{r},t\right)p_i\psi_i\left(\vec{r},\vec{\Omega},t\right)\\&=\frac{\sigma_{si}\left(\vec{r},t\right)}{4\pi}p_i\int_{4\pi}d\vec{\Omega}'\psi_i\left(\vec{r},\vec{\Omega}',t\right)+p_iS_i\left(\vec{r},\vec{\Omega},t\right)+\frac{p_j\psi_j\left(\vec{r},\vec{\Omega},t\right)}{\lambda_j}-\frac{p_i\psi_i\left(\vec{r},\vec{\Omega},t\right)}{\lambda_i}\end{aligned}\tag{14}$$

$$\begin{aligned}&\frac{1}{v}\frac{\partial p_j\psi_j\left(\vec{r},\vec{\Omega},t\right)}{\partial t}+\vec{\Omega}\cdot\vec{\nabla}\left(p_j\psi_j\left(\vec{r},\vec{\Omega},t\right)\right)+\sigma_{tj}\left(\vec{r},t\right)p_j\psi_j\left(\vec{r},\vec{\Omega},t\right)\\&=\frac{\sigma_{sj}\left(\vec{r},t\right)}{4\pi}p_j\int_{4\pi}d\vec{\Omega}'\psi_j\left(\vec{r},\vec{\Omega}',t\right)+p_jS_j\left(\vec{r},\vec{\Omega},t\right)+\frac{p_i\psi_i\left(\vec{r},\vec{\Omega},t\right)}{\lambda_i}-\frac{p_j\psi_j\left(\vec{r},\vec{\Omega},t\right)}{\lambda_j}\end{aligned}\tag{15}$$

$$i,j=1,2\qquad i\neq j\tag{16}$$

This serves as a first-order closure approximation to the unclosed transport equation. As discussed, the LP model is exact in cases of a pure-absorber Markovian-mixing geometry, but loses accuracy with the introduction of non-Poisson statistics in the geometry generation, or with the introduction of angular redistribution in the form of scattering or particle re-emission.

The LP equations are now closed and allow for direct computation of the conditional angular flux ψ_i and ψ_j, among other parameters. One useful parameter may be the unconditional average angular flux $\left\langle \psi\left(\vec{r},\vec{\Omega},t\right)\right\rangle$, computed as shown in equation (17):

$$\left\langle \psi\left(\vec{r},\vec{\Omega},t\right)\right\rangle = p_i\psi_i\left(\vec{r},\vec{\Omega},t\right) + p_j\psi_j\left(\vec{r},\vec{\Omega},t\right) \tag{17}$$

3c. Illustration of Atomic Mix and LP Performance

As an illustration of the properties of the atomic mix and the LP closure models, consider a strongly-absorbing problem subject to the physical parameters in Table 1. These parameters correspond to equal volume fractions of both Material 1 and Material 2, however Material 1 is a very weak pure scattering material, while Material 2 is a correspondingly very strong pure absorbing material. The problem is subjected to an isotropic source of unit magnitude at the left boundary, and a vacuum condition at the right boundary. Under these conditions, we expect the LP model to perform very well due to the strong absorber nature of the problem, but the atomic mix model to perform poorly due to the homogenization effect of removing streaming paths in the problem. These results can be seen in Figure 4a. The exact solution in this figure is the result of an S_{16} diamond-difference transport model applied over 5×10^5 generated realizations.

Parameter	Value
σ_{t1}	$\frac{2}{101}$
σ_{t2}	$\frac{200}{101}$
$\frac{\sigma_{s1}}{\sigma_{t1}}$	1.00
$\frac{\sigma_{s2}}{\sigma_{t2}}$	0.00
λ_1	$\frac{101}{20}$
λ_2	$\frac{101}{20}$

Table 1: A Common Purely Absorbing Material and an Uncommon Purely Scattering Material

Additionally, we may consider a problem with two strongly scattering materials, with parameters seen in Table 2. The results from these parameters may be seen in Figure 4b. For these parameters, the LP closure model is expected to diverge from the true solution due to the introduction of a significant amount of angular redistribution in the form of scattering, providing a memory-effect to the particles in the problem. One can think

of this memory-effect as appearing when the particles are angularly redistributed in a direction opposite to their original flight path, and subsequently see the same materials as they have already traveled through, violating Markovian statistics for that individual particle. In this problem, the atomic mix model will perform better than in the last problem due to there being no obvious streaming avenues available, and the material parameters themselves are closer to the homogenized values than those in the previous problem discussed.

Parameter	Value
σ_{t1}	$\frac{10}{99}$
σ_{t2}	$\frac{100}{11}$
$\frac{\sigma_{s1}}{\sigma_{t1}}$	0.90
$\frac{\sigma_{s2}}{\sigma_{t2}}$	0.90
λ_1	$\frac{99}{100}$
λ_2	$\frac{11}{100}$

Table 2: Two Strongly Scattering Materials

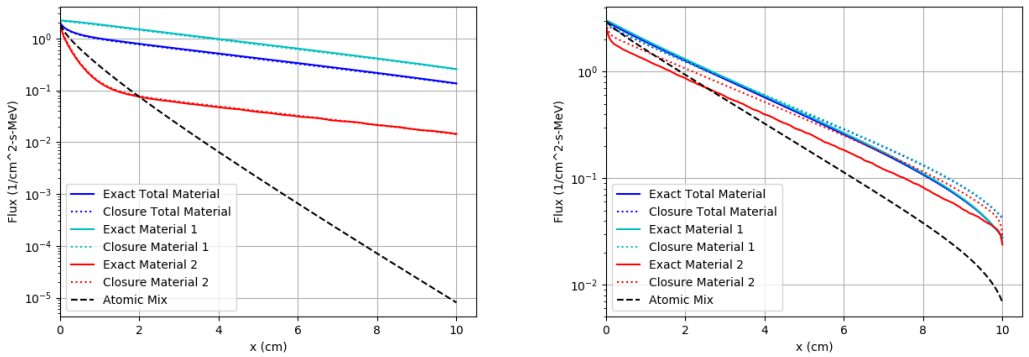

(a) Strongly-Absorbing Profile

(b) Strongly-Scattering Profile

Figure 4: LP vs. Pure Absorber Profiles

4. Thermal Radiation Transport

In the thermal radiation or radiative transport physical regime, the transport equation is tightly coupled to a material energy balance equation, leading to nonlinearities in the transport model. Equation (18) presents the gray radiative transfer equation, while Equation (19) presents the thermal energy balance, resulting in two coupled equations that apply to a stochastically-sampled realization ω. In this equation, I is the angular-dependent intensity value of the radiation, T is the temperature of the medium, c is the speed of light, and a is the radiation constant. The opacity values in the equations are σ_a, σ_s, and σ_t, representing the absorption, effective scattering, and total opacity respectively. The nonlinearities of the equation are present due to the thermal dependence of material values - namely the opacity, density, and specific heat capacity.

$$\frac{1}{c}\frac{\partial I\left(\vec{r},\vec{\Omega},t;\omega\right)}{\partial t}+\vec{\Omega}\cdot\vec{\nabla}I\left(\vec{r},\vec{\Omega},t;\omega\right)+\sigma_t\left(T,\vec{r},t;\omega\right)I\left(\vec{r},\vec{\Omega},t;\omega\right)= \frac{c\sigma_a\left(T,\vec{r},t;\omega\right)}{4\pi}a\left[T\left(\vec{r},t;\omega\right)\right]^4+\frac{\sigma_s\left(T,\vec{r},t;\omega\right)}{4\pi}\int_{4\pi}I\left(\vec{r},\vec{\Omega}',t;\omega\right)d\vec{\Omega}' \quad (18)$$

$$\rho\left(T,\vec{r},t;\omega\right)C_v\left(T,\vec{r},t;\omega\right)\frac{\partial T\left(\vec{r},t;\omega\right)}{\partial t}+c\sigma_a\left(T,\vec{r},t;\omega\right)a\left[T\left(\vec{r},t;\omega\right)\right]^4 = \sigma_a\left(T,\vec{r},t;\omega\right)\int_{4\pi}d\vec{\Omega}'I\left(\vec{r},\vec{\Omega},t;\omega\right) \quad (19)$$

Transforming the thermal radiation transport equations into conditional equations that do not require independent solution over many realizations to produce an ensemble-averaged result involves a similar statistical process of ensemble averaging each term as in the linear transport equation, including the formation of a similar radiation streaming term coupling the two materials in a binary system. This results in the four coupled conditional equations (20) and (21) as transport equations and (22) and (23) as balance equations, governed by the material definition in equation (24):

$$\frac{1}{c}\frac{\partial p_iI_i\left(\vec{r},\vec{\Omega},t\right)}{\partial t}+\vec{\Omega}\cdot\vec{\nabla}p_iI_i\left(\vec{r},\vec{\Omega},t\right)+\sigma_{ti}\left(T_i,\vec{r},t\right)I_i\left(\vec{r},\vec{\Omega},t\right) = \frac{c\sigma_{ai}\left(T_i,\vec{r},t\right)}{4\pi}p_ia\left[T_i\left(\vec{r},t\right)\right]^4+\frac{\sigma_{si}\left(T_i,\vec{r},t\right)}{4\pi}\int_{4\pi}p_iI_i\left(\vec{r},\vec{\Omega},t\right)d\vec{\Omega}'+\frac{p_j\overline{I_j}\left(\vec{r},\vec{\Omega},t\right)}{\lambda_j}-\frac{p_i\overline{I_i}\left(\vec{r},\vec{\Omega},t\right)}{\lambda_i} \quad (20)$$

$$\frac{1}{c}\frac{\partial p_j I_j\left(\vec{r},\vec{\Omega},t\right)}{\partial t}+\vec{\Omega}\cdot\vec{\nabla}p_j I_j\left(\vec{r},\vec{\Omega},t\right)+\sigma_{tj}\left(T_j,\vec{r},t\right)I_j\left(\vec{r},\vec{\Omega},t\right)$$
$$=\frac{c\sigma_{aj}\left(T_j,\vec{r},t\right)}{4\pi}p_j a\left[T_j\left(\vec{r},t\right)\right]^4+\frac{\sigma_{sj}\left(T_j,\vec{r},t\right)}{4\pi}\int_{4\pi}p_j I_j\left(\vec{r},\vec{\Omega},t\right)d\vec{\Omega}'+\frac{p_i\overline{I_i}\left(\vec{r},\vec{\Omega},t\right)}{\lambda_i}-\frac{p_j\overline{I_j}\left(\vec{r},\vec{\Omega},t\right)}{\lambda_j} \tag{21}$$

$$\rho_i\left(T_i,\vec{r},t\right)C_{vi}\left(T_i,\vec{r},t\right)\frac{\partial p_i T_i\left(\vec{r},t\right)}{\partial t}+ac\sigma_{ai}\left(T_i,\vec{r},t\right)p_i\left[T_i\left(\vec{r},t\right)\right]^4$$
$$=\sigma_{ai}\left(T_i,\vec{r},t\right)\int_{4\pi}d\vec{\Omega}'p_i I_i\left(\vec{r},\vec{\Omega},t\right) \tag{22}$$

$$\rho_i\left(T_j,\vec{r},t\right)C_{vj}\left(T_j,\vec{r},t\right)\frac{\partial p_j T_j\left(\vec{r},t\right)}{\partial t}+ac\sigma_{aj}\left(T_j,\vec{r},t\right)p_j\left[T_j\left(\vec{r},t\right)\right]^4$$
$$=\sigma_{aj}\left(T_j,\vec{r},t\right)\int_{4\pi}d\vec{\Omega}'p_j I_j\left(\vec{r},\vec{\Omega},t\right) \tag{23}$$

$$i,j=1,2\qquad i\neq j \tag{24}$$

These equations are, as before, dependent on conditional values of parameters of interest as well as material properties. The values for $\overline{I_i}$ and $\overline{I_j}$ are similarly defined as the conditional ensemble average values of the radiation intensity at the material interface points, which raises a similar closure problem as that highlighted in the linear transport model in that these terms depend on higher-order moments, and cannot be determined simply or *a priori* outside of specific conditions, namely that the geometry is distributed according to Markovian statistics and that there is no angular redistribution of the radiation in the problem. Additionally, the nonlinearities introduced by the thermal dependence of the material properties cannot normally be accounted for, necessitating a method of consistent treatment of the nonlinear terms to study the effect that a heuristic treatment of these nonlinearities has on a system, as explained in the next section of this document.

One important facet to note of the thermal radiation transport equations is that they may themselves be linearized through the use of two assumptions: namely that the material opacity is strictly a function of the cube of the material temperature, and that the material specific heat capacity is strictly a function of the inverse of the cube of the material temperature.

5. Nonlinear Temperature Dependence

While previous work in this area of research has primarily focused on space-dependent models, this section will present a space-independent system for a transport problem. This is motivated by the fact that to date the LP closure is largely applied to stochastic media problems that may be formulated using linear transport equations, which allows for all interaction terms to be expressed in terms of conditionally averaged values without approximation. When the LP closure is applied to a thermal radiative transport problem, where the transport equation is likely to be nonlinear in nature as the absorption and emission terms are functions dependent on temperature, the averaging approach normally applied fails. Averages of nonlinear terms cannot be expressed in terms of the average temperature in each material, resulting in a secondary closure problem due to temperature itself being a stochastic term. A purely time-dependent model renders the LP closure exact, such that the effects of nonlinearities may be precisely established and studied.

To establish this model, consider a spatially homogeneous geometry, effectively comprised of a single cell such that all temporal effects are felt instantaneously within the system. This may be conceived of as a subvolume within a large computational domain. As time progresses, the material comprising the system will switch between two states subject to Poisson statistics in time. This is similar to the spatial realizations visualized in Figures 2 and 3, however the unit of propagation is temporal as opposed to spatial.

Coupled nonlinear equations of radiation intensity I and temperature T for a time-dependent space-independent transport model for gray radiation can be written as a function of the material state ω, seen in equations (25) and (26). Material properties include density ρ, specific heat C_v, and opacity σ_a. The spatially-independent nature of this problem statement renders any angular redistribution within the problem physics as a non-issue.

$$\frac{1}{c}\frac{\partial I\left(t;\omega\right)}{\partial t}+\sigma_a\left(T,t;\omega\right)I\left(t;\omega\right)=c\sigma_a\left(T,t;\omega\right)aT^4\left(t;\omega\right) \tag{25}$$

$$\rho\left(T,t;\omega\right)C_v\left(T,t;\omega\right)\frac{\partial T\left(t;\omega\right)}{\partial t}+c\sigma_a\left(T,t;\omega\right)aT^4\left(t;\omega\right)=\sigma_a\left(T,t;\omega\right)I\left(t;\omega\right) \tag{26}$$

These equations are subject to nonrandom initial conditions, seen in equation (27):

$$I\left(0;\omega\right)=I_0,\quad T\left(0;\omega\right)=T_0 \tag{27}$$

It should be noted that while this model does exactly preserve the temperature nonlinearity within a stochastic temporal model, it is not necessarily representative of any particular physical phenomena. The primary reason for this is in the characteristics of the model: radiation intensity and material temperature are both preserved across material transitions, while only material properties are stochastic in time. While radiation intensity is simple to conceptually apply as a conserved quantity, it is difficult to conceive of a physically occurring system where temperature is instantaneously conserved between two materials on a radiative transport time-scale, regardless of which material currently occupies the spatially homogeneous system.

However, due to the preservation of both intensity and temperature, these quantities may be obtained exactly as first-order moments. By defining the intensity and temperature within a given realization as ϕ and θ respectively, these moment equations may be written in terms of the probability density $P_i(\phi, t)$ that ϕ lies in the range $(\phi, \phi + d\phi)$ conditioned on the material at time t being i, and the probability density $P_i(\theta, t)$ that θ lies in the range $(\theta, \theta + d\theta)$ conditioned on the material at time t being i, respectively. These moment equations are shown in equations (28) and (29):

$$\phi_i(t) = \int_0^\infty \phi P_i(\phi, t)\, d\phi \tag{28}$$

$$\theta_i(t) = \int_0^\infty \theta P_i(\theta, t)\, d\theta \tag{29}$$

Note that closed equations for the moments defined above cannot be written down for the case of nonlinearity in the temperature-dependent physical properties, but may be correctly and exactly established for the linearized case. These model equations may be solved using a numerical method involving realization generation and Newton iteration, as well as using a state-based stochastic method that is explicit in time.

5a. Implicit Numerical Solution

An implicitly defined and robust numerical solution may be applied to individually generated temporal realizations. This solution begins with the application of the Backward Euler approximation to the model equations defined in equations (25) and (26), with individual time-step values over a discretized time domain being represented by the index n. The result can then algebraically be set equal to zero and expressed as a function of intensity and temperature, as shown in equations (30) and (31).

$$\phi_{n+1} - \Delta t c^2 \sigma_a \left(\theta_{n+1}\right) a\theta_{n+1}^4 + \Delta t c \sigma_a \left(\theta_{n+1}\right) \phi_{n+1} - \phi_n = 0 \tag{30}$$

$$\theta_{n+1} - \frac{\Delta t \sigma_a \left(\theta_{n+1}\right)}{\rho \left(\theta_{n+1}\right) C_v \left(\theta_{n+1}\right)} \phi_{n+1} + \frac{\Delta t c \sigma_a \left(\theta_{n+1}\right)}{\rho \left(\theta_{n+1}\right) C_v \left(\theta_{n+1}\right)} a\theta_{n+1}^4 - \theta_n = 0 \tag{31}$$

The details of a realization are provided by the allocation of an unstructured array of arbitrary size determined at the time of realization generation. The first material within the realization is sampled from the temporal occupation fraction of each material, which must be defined within the problem parameters. This temporal occupation fraction is conceptually similar to a volume fraction, however applied to temporal coordinates as opposed to spatial coordinates.

By defining each segment of any contiguous material as a sublayer, the methodology utilized to construct an independent realization can be described as discretizing each sublayer into a set number of time points, after which the next sublayer generated is discretized into the same number of time points. This repeats until the specified completion time for the problem is reached, upon which the last sublayer generated is truncated to the completion time, and then discretized into the same set number of time points. This generation-and-discretization scheme prevents solving the transport equation at a condition where a material transition occurs in the midst of a time-step, which if it were to happen, would reinstate a closure problem within the discretized cell of the problem domain. As these discretizations are of arbitrary temporal width Δt, determined at the time of sampling the temporal sublayer duration, the results of the transport model must be mapped onto a structured overlay grid that will be used to define the conditionally averaged quantities of interest for the problem.

The unstructured to structured discretization conversion is accomplished by using time-duration weights on the values computed at the unstructured time points to obtain time-duration weighted values at the structured time points of interest. This process by necessity results in the inclusion of "partial values" induced by material transitions occurring in the middle of a structured time-step. These partial values preserve the mean quantity of the parameter in question, but introduce notable statistical error into the solution.

5b. Stochastic Simulation Algorithm

A stochastic simulation algorithm is developed as an alternative to the direct numerical solution, which bypasses the requirement to generate temporal realizations on which to

solve the transport equations, and instead defines a sampling scheme across a structured discretization profile without the need for any mapping process to occur. This algorithm can be derived by stating that: within a sufficiently small but finite time duration Δt, two mutually exclusive events may occur, those being either a material transition or the absence of a material transition. In the case of the latter event, the internal state of the system is propagated according to the physical parameters of radiation transport.

The probability of a material transition is shown in equation (32):

$$P\left(i \to j\right) = \frac{\Delta t}{\tau_i} \tag{32}$$

Alternatively, the internal state of the system, comprised of radiation intensity I and material temperature T will change subject to the probability shown in equation (33):

$$P\left(\neg\left(i \to j\right)\right) = 1 - \frac{\Delta t}{\tau_i} \tag{33}$$

These probabilities depend on a mean sojourn time τ_i of material i, defined as the average amount of time that the state of the system is comprised of material i before changing. This is comparable to the mean chord length of a spatially stochastic system, but applied to temporal coordinates, with a similar relation to the temporal occupation fraction. The probability of an internal state change occurring concurrently with a material transition is $O\left(\Delta t^2\right)$, and subsequently ignored as inconsequential given a sufficiently small value of Δt.

In the event that an internal state change occurs, the governing equations may be deterministically derived from the use of the forward Euler approximation on equations (25) and (26), the results of which are shown in equations (34) and (35):

$$I\left(t + \Delta t\right) - I\left(t\right) = \Delta t\left(c^2 \sigma_a\left(T\right) aT\left(t\right)^4 - c\sigma_a\left(T\right) I\left(t\right)\right) \tag{34}$$

$$T\left(t + \Delta t\right) - T\left(t\right) = \frac{\Delta t}{\rho\left(T\right) C_v\left(T\right)}\left(\sigma_a\left(T\right) I\left(t\right) - c\sigma_a\left(T\right) aT\left(t\right)^4\right) \tag{35}$$

As with the realization generation method, the initial material present in any given history of the system is sampled from the temporal occupation fraction of the two materials. Following the determination of the initial material, the above described probabilities are sampled within each discrete time-step, determining either a material transition or an internal state change within that time-step, accompanied by a time propagation of Δt until the specified completion time of the problem is reached. Many such histories

are computed, the results of which are used to obtain conditionally averaged values for material properties of interest. By nature of these solution statements, one stochastic simulation history is directly comparable to one temporal realization generated for the direct implicit numerical solution.

5c. Heuristic Model for Material Averages

Within the definition of the temporally-varying problem, it is noted that the statistics of the material mixing and solution dynamics are jointly Markovian, thereby rendering the Levermore-Pomraning closure model exact. However, the material properties within such a closure model must be represented as functions of the average temperature. Coupled equations for the radiation intensity transport and material energy balance in the heuristic extension of the temporal problem are shown below in the coupled equations (36), (37), (38), and (39):

$$\frac{dp_i I_i(t)}{dt} = c^2 \sigma_{ai}(T_i, t)\, a p_i \left[T_i(t)\right]^4 - c\sigma_{ai}(T_i, t)\, I_i(t) + \frac{p_j I_j(t)}{\tau_j} - \frac{p_i I_i(t)}{\tau_i} \tag{36}$$

$$\frac{dp_j I_j(t)}{dt} = c^2 \sigma_{aj}(T_j, t)\, a p_j \left[T_j(t)\right]^4 - c\sigma_{aj}(T_j, t)\, I_j(t) + \frac{p_i I_i(t)}{\tau_i} - \frac{p_j I_j(t)}{\tau_j} \tag{37}$$

$$\frac{dp_i T_i(t)}{dt} = \frac{1}{\rho_i(T_i, t)\, C_{vi}(T_i, t)} \left(\sigma_{ai}(T_i, t)\, I_i(t) - c\sigma_{ai}(T_i, t)\, a p_i \left[T_i(t)\right]^4\right) + \frac{p_j T_j(t)}{\tau_j} - \frac{p_i T_i(t)}{\tau_i} \tag{38}$$

$$\frac{dp_j T_j(t)}{dt} = \frac{1}{\rho_j(T_j, t)\, C_{vj}(T_j, t)} \left(\sigma_{aj}(T_j, t)\, I_j(t) - c\sigma_{aj}(T_j, t)\, a p_j \left[T_j(t)\right]^4\right) + \frac{p_i T_i(t)}{\tau_i} - \frac{p_j T_j(t)}{\tau_j} \tag{39}$$

These equations, due to the jointly Markovian physics, allow for the isolation of the error introduced by the closure terms in both the radiation intensity and material temperature. The solution to the heuristic model can be developed similarly to the direct numerical simulation via a discretization scheme, but without the need for generating individual realizations.

5d. Radiation Loss

In addition to the models for an equilibrium case, an ad-hoc approach to accounting for a loss of radiation or leakage to the problem domain has also been implemented. This is effectively a simple additional term in the radiation transport equation of the system as seen in equation (25), which now looks as shown in equation (40):

$$\frac{1}{c}\frac{\partial I\left(t;\omega\right)}{\partial t}+\alpha\sigma_{a}\left(T,t;\omega\right)I\left(t;\omega\right)=c\sigma_{a}\left(T,t;\omega\right)aT^{4}\left(t;\omega\right) \tag{40}$$

Due to the lack of physical data for the specific time-dependent problem as described herein, the leakage takes the form of a simple modifier folded with the absorption term in the problem, denoted as α. Any value of α greater than unity will effectively siphon radiative energy from the system, approximating the effect that a constant leakage term would have. The solution equations are modified accordingly, with the simple product of this destruction factor on the radiation absorption terms within each model.

5e. Numerical Results

As a presentation of a comparison of the implicit numerical method and the explicit stochastic simulation algorithm, consider a case where the only material property that varies as a function of temperature is opacity, subject to equation (41):

$$\sigma_{ai}\left(T\right)=\frac{A_{i}}{T^{3}} \tag{41}$$

The constants defined for each material are as follows: $A_1 = 1.0$ eV^3 cm^{-1}, $A_2 = 5.0$ eV^3 cm^{-1}, $\tau_1 = 3.35 \times 10^{-14}$ s, $\tau_2 = 1.67 \times 10^{-13}$ s, $\rho_1 = \rho_2 = 1.0$ g cm^{-3}, $C_{v1} = C_{v2} = 1.0$ erg g^{-1} eV^{-1}. The initial values of the problem are defined as: $I_0 = 1.0$ erg cm^{-2} s^{-1}, and $T_0 = 1.0$ eV. The selected initial conditions of the problem describe a system with a relatively small amount of initial radiative energy and a relatively large amount of initial material temperature, such that the dynamics of the problem involve a transition of thermal energy into radiative energy. The selected end time of the problem is 10^{-11} seconds. Note that time may be multiplied by the constant speed of light value c to be of a more reasonable magnitude. The radiation intensity profiles of the implicit numerical method and the explicit stochastic simulation algorithm may be seen in Figure 5. For both the numerical and stochastic simulation algorithms, the number of time-steps utilized was 10^3. The direct numerical simulation method computed 10^5 realization and averaged the results, while the stochastic simulation method computed

10^5 histories and averaged the results. For the sake of comparison, the profile obtained by solving the atomic mix model as well as the heuristic model with the same parameters is also shown in each figure.

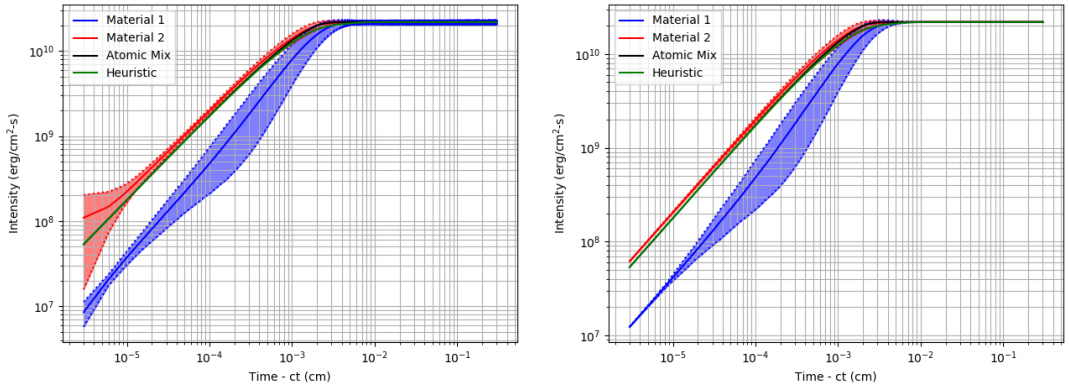

(a) Direct Numerical Experiment (b) Stochastic Simulation

Figure 5: Radiation Intensity Profiles

Within the profiles, it can be seen that the statistical noise accrued during the unstructured to structured discretization mapping method is visible in the results. The most visible location on the intensity profile is towards the lower time values of the profile, where the magnitude is smaller and the relative visual difference is heightened by the logarithmic scale of the figures. The standard deviation shown by the stochastic simulation method is largely attributed to that introduced by the inherent stochasticity of the problem, until the system has existed for a long enough period of time to reach an equilibrium value between radiative energy and thermal energy due to the lack of energy loss terms present in the system. This same standard deviation trend in stochasticity is present in the numerical solution, and is much larger in relative scale to the noise produced by the mapping process. Similar effects are seen in Figure 6 for the temperature profiles of the numerical method and the stochastic simulation method. As before, these profiles also contain the atomic mix model and heuristic model solutions.

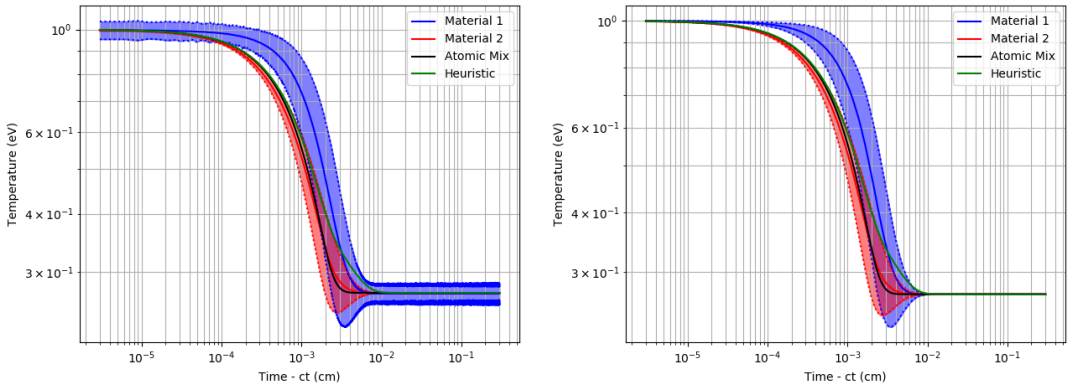

(a) Direct Numerical Experiment (b) Stochastic Simulation

Figure 6: Temperature Profiles

It should be noted that the standard deviation computed from the square root of the variance is assumed symmetric about the mean trend line in each profile, which may not necessarily reflect reality. That is, it is considered to be physically improbable that the temperature profile of any given material realization of history will undershoot the equilibrium value between radiation and material energy, but rather once equilibrium value is reached it can be assumed that any deviation from that value is unphysical.

The performance of the stochastic simulation algorithm in comparison to the direct implicit numerical solution is consistently drastically improved. Specifically, the implicit numerical solution takes approximately 70 times more compute time to complete than does the stochastic simulation algorithm.

By setting the value of α, the radiation destruction factor that is used as a multiplier on the absorption terms in the equations, to a value of 1.5, the profiles seen in Figure 7 are produced. The resultant ensemble averaged profiles from both the stochastic simulation algorithm and the numerical solution are essentially identical, and visually indistinct.

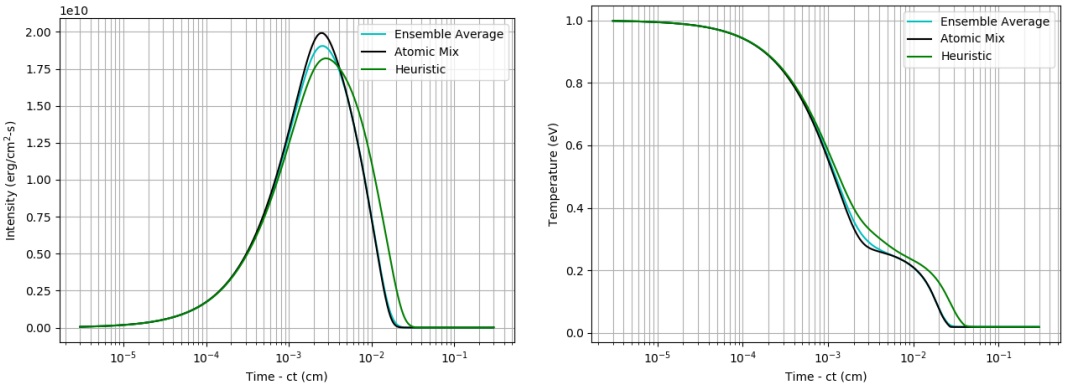

(a) Intensity with Loss

(b) Temperature with Loss

Figure 7: Parameter Profiles with Radiation Loss

5f. Probability Densities

In addition to the low order moments of parameters of interest for this system, the values at a specific time step of individual realizations or histories may be tallied to construct a histogram profile, which can then be normalized into a probability density function in the form of a curve. The process for computing these profiles includes a first-pass of the problem to establish the minimum and maximum values seen such that histogram bins may be produced, and then a second-pass to fill the bins with tallies and produce a probability density function curve. The results of taking these tallies at a time-step that is just short of the equilibrium location for the general case, and a time-step that is near the peak intensity profile for the case with the ad-hoc leakage adjustment, are shown in Figures 8, 9, and 10. These are relatively rough profiles due to the computationally intensive nature of construction, computed from ten histogram bins each.

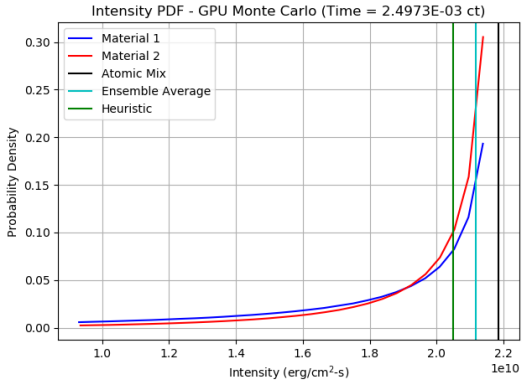

(a) Intensity PDF

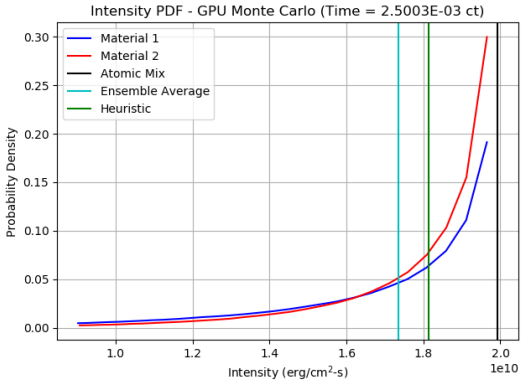

(b) Intensity PDF with Loss

Figure 8: Intensity Probability Density Functions

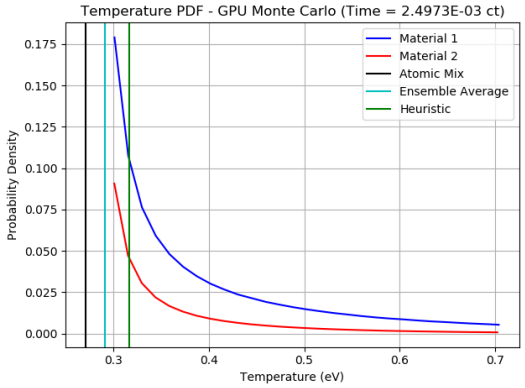

(a) Temperature PDF

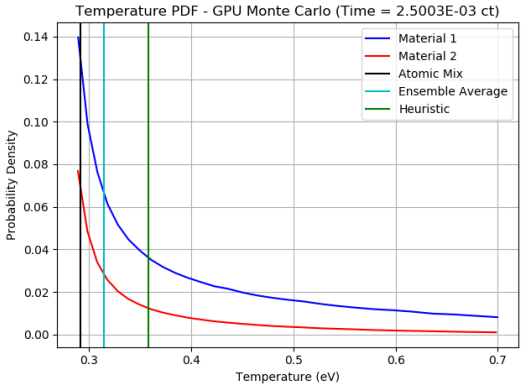

(b) Temperature PDF with Loss

Figure 9: Temperature Probability Density Functions

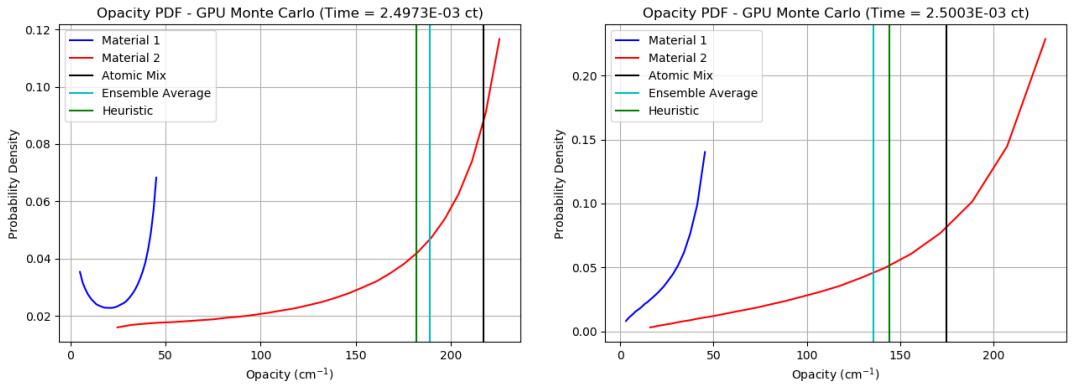

(a) Opacity PDF

(b) Opacity PDF with Loss

Figure 10: Opacity Probability Density Functions

These profiles also include the results of the heuristic model, as well as the atomic mix model for comparison. The blue line indicating the ensemble average results are those that are obtained from computing the ensemble average mean value at that location in time from both materials.

A direct calculation of the probability density functions is also possible. Applying the principle of conservation of probability to the Markovian system yields exactly closed equations for the joint conditional probability density $P_i(\phi, \theta, t)\, d\phi d\theta$, which is the probability that the radiation intensity lies in the range $(\phi, \phi + d\phi)$ and that the temperature lies in the range $(\theta, \theta + d\theta)$, conditioned on the material being material i. These equations can be seen below, as equations (42) and (43):

$$\frac{\partial}{\partial t}(p_1 P_1) + \frac{\partial}{\partial \phi}(f_1 p_1 P_1) + \frac{\partial}{\partial \theta}(g_1 p_1 P_1) = \frac{p_2}{\tau_2} P_2 - \frac{p_1}{\tau_1} P_1 \tag{42}$$

$$\frac{\partial}{\partial t}(p_2 P_2) + \frac{\partial}{\partial \phi}(f_2 p_2 P_2) + \frac{\partial}{\partial \theta}(g_2 p_2 P_2) = \frac{p_1}{\tau_1} P_1 - \frac{p_2}{\tau_2} P_2 \tag{43}$$

The functions f_i and g_i are defined as in equations (44) and (45):

$$f_i(\phi, \theta) = c\sigma_{ai}(\theta)\left(ca\theta^4 - \phi\right) \tag{44}$$

$$g_i(\phi, \theta) = \frac{\sigma_{ai}(\theta)}{\rho_i C_{vi}(\theta)}\left(\phi - ca\theta^4\right) \tag{45}$$

These equations will be solved and benchmarked against histogram profiles generated from the efficient stochastic simulation algorithm. Possible numerical solution methodologies are the utility of a backward Euler approximation in time, or the application

of finite difference or finite element methods in the intensity and temperature profiles. There may be a heuristic closure model for non-Markovian switching that possible to incorporate and study, but that is very much dependent on the time remaining within this research deadline.

6. Implicit Monte Carlo Implementation in Branson

Monte Carlo methods use stochastic sampling to determine how and where a model particle moves through a system, and through the laws of large numbers are able to approximate a general solution to a complicated or multi-dimensional system. Monte Carlo methods typically come at the expense of a long run-time, and have a standard convergence criteria proportional to $\frac{1}{\sqrt{N}}$, where N is the number of histories computed.

The Implicit Monte Carlo (IMC) method of representation of the thermal radiative transport equations relies on an $O(\Delta t)$ approximation on the thermal emission of the physics, as seen in equation (46), given a time-step n, resulting from a Taylor series expansion in $\Delta t = t - t_n$ about t_n:

$$T_{n+1}^4 = T_n^4 + 4\Delta t T_n^3 \frac{\partial T}{\partial t} + O\left(\Delta t^2\right) \tag{46}$$

This results in a need for an effective scattering approximation [10] to represent particle absorption and re-emission within the current time-step, denoted by the so-called Fleck factor f, seen in equation (47):

$$f = \frac{1}{1 + \frac{4acT^3\sigma_a\Delta t}{\rho C_v}} \tag{47}$$

The thermal radiative transport equations are then expressed as in equations (48) and (49):

$$\frac{1}{c}\frac{\partial I\left(\vec{r},\vec{\Omega},t\right)}{\partial t} + \vec{\Omega}\cdot\vec{\nabla}I\left(\vec{r},\vec{\Omega},t\right) = \frac{f}{4\pi}c\sigma_a\left(T,\vec{r}\right)a\left[T\left(\vec{r},t\right)\right]^4 + \frac{1-f}{4\pi}\int_{4\pi} d\vec{\Omega}'\sigma_a\left(T,\vec{r}\right)I\left(\vec{r},\vec{\Omega}',t\right) \tag{48}$$

$$\rho\left(T,\vec{r}\right)C_v\left(T,\vec{r}\right)\frac{\partial T\left(\vec{r},t\right)}{\partial t} + fc\sigma_a\left(T,\vec{r}\right)a\left[T\left(\vec{r},t\right)\right]^4 = f\sigma_a\left(T,\vec{r}\right)\int_{4\pi} d\vec{\Omega}' I\left(\vec{r},\vec{\Omega}',t\right) \tag{49}$$

The thermal radiation transport equations are linearized by the use of a semi-implicit time discretization, by virtue of which IMC is subject to a maximum principle stability limit, restricting the spatial mesh and temporal discretization limits. If the maximum principle stability limit is violated, unphysical behavior results, in particular the existence of temperatures within the problem domain that are larger than a source temperature.

A simple Cartesian-coordinate IMC implementation called Branson has been written by Alex Long at Los Alamos National Laboratory [11], and serves as a basis for stochastic media experiment development in an IMC context. Branson uses standard IMC transport algorithms [12] to trace particles, track radiation fluence and material parameters, and output data in a readable and post-processable uniform format.

Branson previously utilized only vacuum and reflective boundary conditions, with additional bookkeeping conditions used for managing photon transport between computational ranks in the context of parallel processing. Certain problems of interest involve a large amount of incident radiation on initially cold media, wherein radiation is transported through the media as a Marshak wave [13]. Such problems are modeled easily with a boundary condition capable of generating isotropic photon packets from a set temperature. To this end, a source boundary condition option has been made available, which includes a temperature value as input. This boundary condition generates work packets of photons at the boundary face of the problem, with additional logic for separating the photon transport workload between computational ranks for parallel computation.

Due to the high volume of comptutational work required for modeling stochastic media via geometry generation, a method that requires only one iteration of transport calculation may be preferred for problem modeling. The chord length sampling method creates a probability distribution function that describes the distribution of different materials within a stochastic mixture, comparable to that of the LP closure model [8]. During photon transport, the distribution is used to sample a probable location at which the photon packet will transition to a new material. If that distance is shorter than the distance to the next interaction, it is assumed that the photon packet transitions materials at the sampled distance. This method assumes that every segment of a photon history is uncorrelated, which means that in problems with a relatively large amount of scattering or effective scattering interactions, photons that are back-scattered toward a sampled material will no longer see the same material as it was known to the photon previously. This method will be accurate for pure-absorber problems, but less so for media that incorporate scattering physics.

As a comparison, consider a problem with densities and specific heats set to unity. The constant value of σ_1 is 90.1, the constant value of σ_2 is 0.10, the value of λ_1 is 0.11, and the value of λ_2 is 0.99. The atomic mix results are shown in Figure 11, the chord length sampling results in Figure 12, and the realization generation in Figure 13.

A model of one-dimensional geometry is set up within a three-dimensional IMC pro-

gram by taking advantage of reflective boundary conditions. A columnar geometry in Cartesian coordinates is used, with subsequent segments extending the x-direction. Both boundary conditions in the y-direction are reflecting, and both boundary conditions in the z-direction are reflecting, allowing for the geometry to be mathematically equivalent to a planar medium. The volumetric nature of certain properties such as the material specific heat is offset by the balance of the transport equations themselves, wherein a balance between the absorption of radiation contributing to the temperature of the material and the emission of radiation dependent on material temperature exists independent of volume within a columnar segment of dx subject to reflective boundary conditions in y and z.

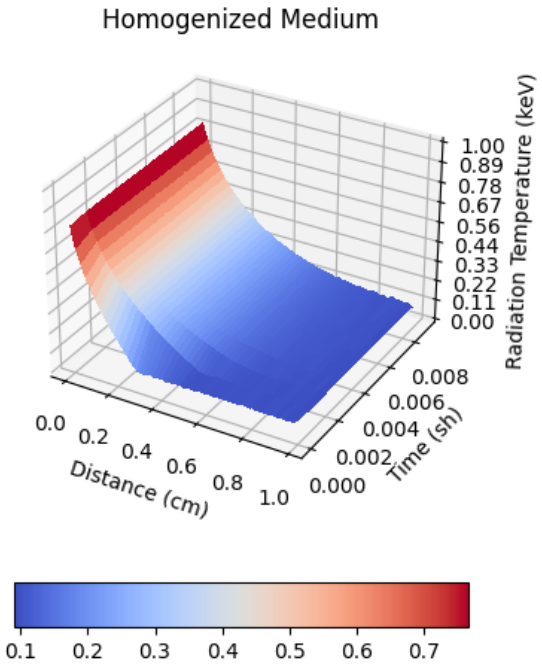

Figure 11: Homogeneous 1D IMC Problem

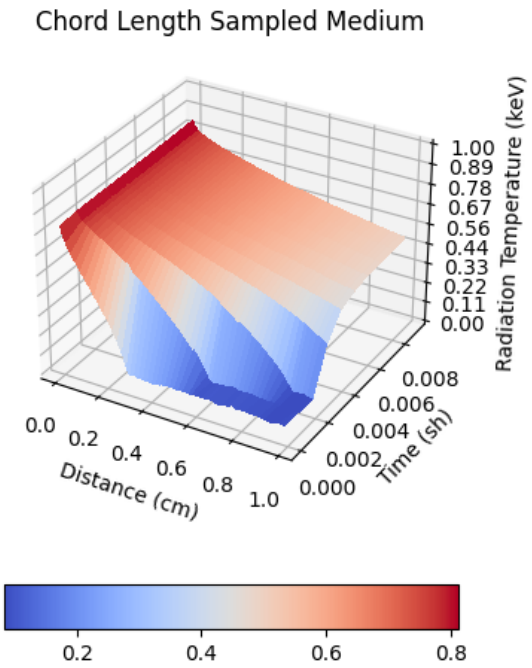

Figure 12: Chord Length Sampling 1D IMC Problem

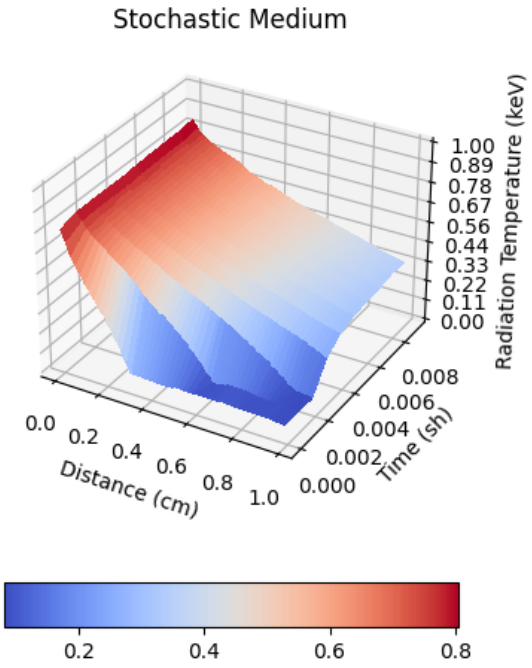

Figure 13: Stochastic Geometry 1D IMC Problem

Material temperature profiles are not shown for these cases because both the radiation and the material temperature are initially set to 0.1 keV, and so they differ very little from the radiation temperature profiles and offer no additional visual information. The Marshak wave is propagating much more rapidly in the stochastic medium case, as there are large portions of the problem that allow free streaming of the radiation due to the optically thin material being the majority of the problem volume fraction. Once the radiation reaches an optically thick sublayer, it possesses the majority of the energy it had at the surface source (1 keV), and is able to deposit a large amount in the optically thick material regardless of where it appears in the problem. However, the wave in question is radiation temperature, which is most likely influenced primarily by the radiation streaming to the boundary directly from the source rather than re-emission from the materials, simply due to the mean chord length selected for the optically thin material which occupies the entire problem domain. In the case of the homogenized medium, the Marshak wave is propagating according to expected models but with much more attenuation in radiation temperature. In this case, the exponential attenuation of energy on each photon packet is constant and appreciable, and so towards the problem boundary the photon possesses markedly less energy if it was not absorbed.

The chord length sampling method performs similarly to the realization generation method, allowing for more particle streaming through optically thin regions of space than seen in the atomic mix results. In this case, the equilibrium temperature of the system at the vacuum boundary is higher in the chord length sampling method than in the realization generation method. This is likely due to previous streaming paths known to the particle no longer existing after an interaction involving angular re-distribution. This ultimately results in particles that have streamed through a section of the domain not often making the return trip if back-scattered, and being scattered or re-emitted later in the problem domain than would be possible in the realization generation method. The result is that the realization generation method keeps particles traveling within the domain for longer due to the existence of set streaming paths, resulting in more effective attenuation.

6a. Poisson Box Generation

Planned work is to expand the geometry generation in Branson to include two-dimensional models through the use of Poisson Box tessellations [7]. A Poisson Box tesselation consists of a two-dimensional domain wherein both the x and y dimensions are randomly

intersected with a number of planes sampled according to the box density ρ_b, seen in equation (50):

$$\rho_b = \frac{2}{3\lambda_c} \tag{50}$$

This relationship depends on the correlation length of the system, itself a Markovian statistical parameter, defined as seen in equation (51):

$$\lambda_c = \left(\frac{1}{\lambda_1} + \frac{1}{\lambda_2}\right)^{-1} \tag{51}$$

The planes that bisect each axis are placed randomly according to a uniform distribution across the domain equivalent to the length of the overall problem domain along that axis. As random unstructured Cartesian boxes are constructed in the domain, they are then randomly assigned a material by sampling uniformly from the volume fraction of each material, in a process known as "coloring". Examples can be seen in Figure 14 and Figure 15.

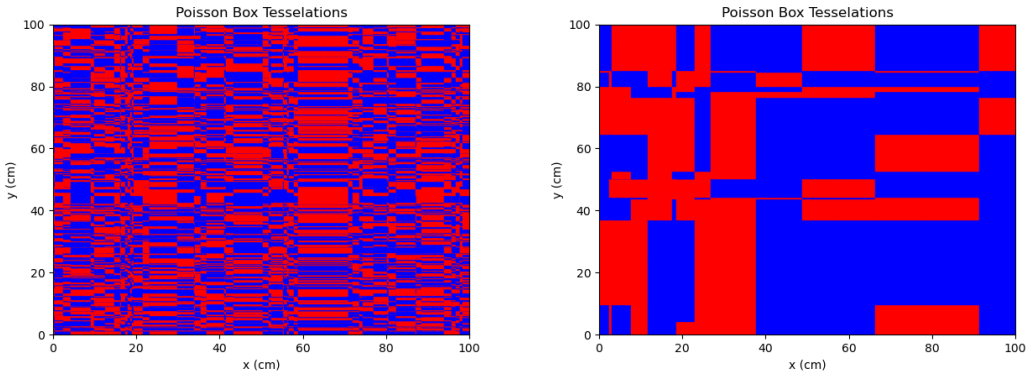

Figure 14: Independent 2D Poisson-Box Realizations of $\lambda_1 = \frac{101}{20}$ cm [blue], $\lambda_2 = \frac{101}{20}$ cm [red]

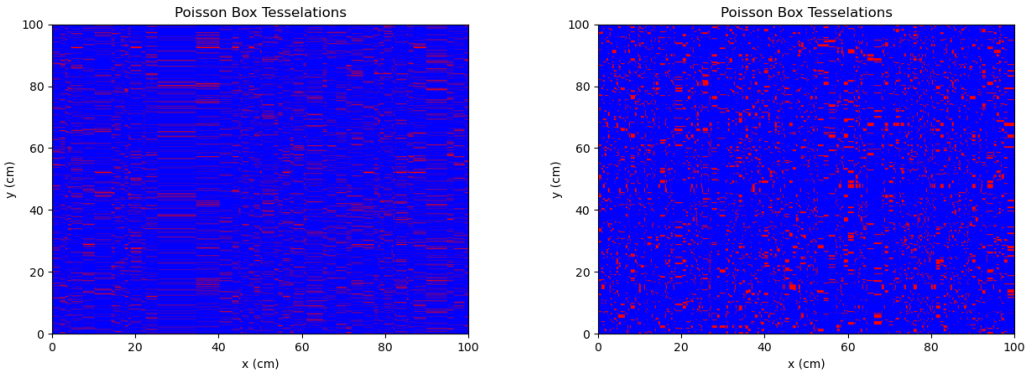

Figure 15: Independent 2D Poisson-Box Realizations of $\lambda_1 = \frac{99}{100}$ cm [blue], $\lambda_2 = \frac{11}{100}$ cm [red]

Due to the similarities of Poisson Box tessellations with Markovian distributions [7], such generation methodologies yield comparable results to stochastic Markovian physics. By incorporating such two-dimensional geometries, it is planned to assess the Markovian closure accuracy in two dimensions relative to one dimension. Additionally, diffusion limits of chord length sampling solutions as well as realization generation methodologies will be investigated in both 1D and 2D regimes.

7. Non-Markovian Closure Model

This section may be considered ancillary to the bulk of this document, and may be restricted in analysis by time constraints of the current research project.

Efforts to develop an effective and efficient alternative to the LP model that performs as well, or better, in systems with non-Markovian effects are underway. In particular, systems with stochastic geometries that are not described by Markovian mixing statistics are not accurately described by the LP model. Additionally, any amount of particle scattering introduces a non-Markovian element to the system by incorporating memory effects into the particle transport.

For simplification, equations (10) and (11) are written for monoenergetic, steady-state, one-dimensional slab geometry, where $\mu = \cos(\theta)$ and θ is the directional angle from the x-axis that a particle travels, resulting in equations (52) and (53):

$$\mu \frac{\partial p_i \psi_i(x,\mu)}{\partial x} + \sigma_{ti}(x)\, p_i \psi_i(x,\mu) = \frac{\sigma_{si(x)}}{2} \int_{-1}^{1} d\mu' p_i \psi_i(x,\mu') + |\mu| \left(\frac{p_j}{\lambda_j} \overline{\psi}_j(x,\mu) - \frac{p_i}{\lambda_i} \overline{\psi}_i(x,\mu) \right) \quad (52)$$

$$\mu \frac{\partial p_j \psi_j(x,\mu)}{\partial x} + \sigma_{tj}(x)\, p_j \psi_j(x,\mu) = \frac{\sigma_{sj(x)}}{2} \int_{-1}^{1} d\mu' p_j \psi_j(x,\mu') + |\mu| \left(\frac{p_i}{\lambda_i} \overline{\psi}_i(x,\mu) - \frac{p_j}{\lambda_j} \overline{\psi}_j(x,\mu) \right) \quad (53)$$

Whereas the LP model makes the substitution that $\overline{\psi}_i = \psi_i$, the alternative use of a memory kernel via an operator $\mathcal{K}$ to capture non-Markovian effects in a one-dimensional system of domain D is proposed, seen in equation (54):

$$\overline{\psi}_i = \mathcal{K}\psi_i = \int_{-1}^{1} d\mu' \int_D dx' K(x' \to x; \mu' \to \mu)\, \psi_i(x', \mu') \quad (54)$$

A heuristic representation of $\mathcal{K}\psi_i$ has been chosen with a peaked memory kernel for study, seen in equation (55):

$$\mathcal{K}\psi_i = \eta \psi_i(x,\mu) - \operatorname{sgn}(\mu)\, \gamma \frac{\partial}{\partial x} \psi_i(x,\mu) \quad (55)$$

Equation (55) introduces a memory parameter γ that governs the degree of influence of the non-Markovian parameters of the system, as well as a Markovian parameter η

that allows for the Markovian closure model terms to be present at varying intensities. The sgn (μ) function present in equation (55) is necessary to preserve the symmetry of the solution, as the first-order derivative term is direction-dependent.

Due to the fact that the memory effects are governed by the derivative terms in the heuristic closure model, the representation of these effects is very localized. An example illustrating this behavior may be seen by computing the solution to a high-contrast mix problem subject to the parameters in Table 3. For ease of developing solutions and as an ad-hoc approach to determining values of γ, the correlation length λ_c of the two materials is used as a basis. The correlation length is a parameter specific to Markovian-geometry problems, and may be computed in a binary material by the methodology seen in equation (56):

$$\lambda_c = \left(\frac{1}{\lambda_1} + \frac{1}{\lambda_2}\right)^{-1} \tag{56}$$

An important facet of γ in equation (55) is that to allow for standard transport solution methodology to be appropriate, the value of γ may not exceed λ_c in the general case. This allows for the combined streaming term to always be of the same sign as μ in the resulting transport equation. This is not a physical or mathematical limit, however extra care must be taken in cases when $\gamma > \lambda_c$.

Parameter	Value
λ_1	$\frac{99}{10}$
λ_2	$\frac{11}{10}$
σ_1	$\frac{10}{99}$
σ_2	$\frac{100}{11}$
γ	$\frac{2}{3}\lambda_c$
η	1

Table 3: High-Contrast Mix

Independent material solutions for an isotropic flux of unity at the left boundary and a vacuum condition at the right boundary may be seen in Figure 16, where the benchmark solution by the generation of 5×10^6 geometries is represented in green. The LP model is represented in red, and the non-Markovian closure model, denoted "NM", is represented in blue. Note that there is an expected boundary layer in Material 2, due to the physical parameters of the system. Particles that spawn in Material 2 very rapidly transition out of Material 2 due to the small volume fraction of that material. This boundary layer

is where the performance of the non-Markovian model shows improvement over that of the LP model. However, in this case the model corrects itself to approximating the LP solution for the majority of the problem domain.

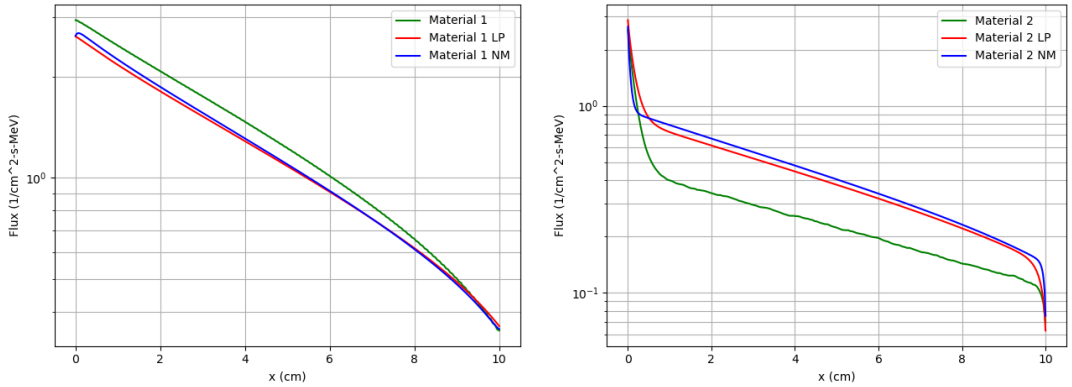

(a) Material 1 Profiles (b) Material 2 Profiles

Figure 16: High-Contrast Mix Profiles

A low-contrast mix is also studied, subject to the values in Table 4. While the value for gamma remains the same as that for the high contrast mix, improvement in the solution within the domain of the problem can be seen by adjusting the value of η.

Parameter	Value
λ_1	3.00
λ_2	1.00
σ_1	1.00
σ_2	5.00
γ	$\frac{2}{3}\lambda_c$

Table 4: Low-Contrast Mix

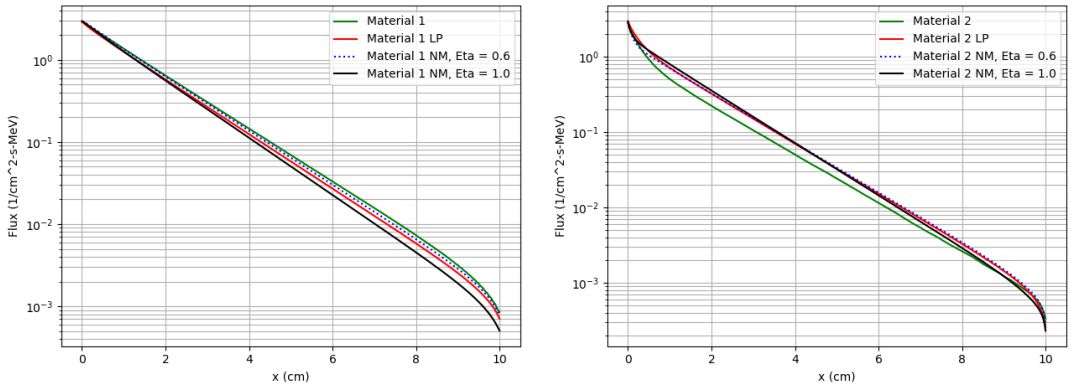

(a) Material 1 Profiles

(b) Material 2 Profiles

Figure 17: Low-Contrast Mix Profiles

Further efforts to characterize a non-Markovian closure model are required. To this end, a strong-memory approximation is proposed, seen in equation (57):

$$\mathcal{K}\psi_i = \eta\psi_i\left(x,\mu\right) - \operatorname{sgn}\left(\mu\right)\gamma\frac{\partial}{\partial x}\psi_i\left(x,\mu\right) + \int_D dx' K\left(x'\to x\right)\phi_i\left(x'\right) \tag{57}$$

In the above equation, K is the memory kernel denoting the effects of systemic memory on the transport solution. One possible selection for a kernel would be an exponential parameterized kernel, shown in equations (58) and (59):

$$K\left(x'\to x\right) = \frac{k_0}{\beta}\exp\left(-\frac{|x-x'|}{\beta}\right) \tag{58}$$

$$\beta = \frac{1}{k_0}\int_0^\infty xK\left(x\right)dx \tag{59}$$

The above equations have a purely theoretical basis for the exponential memory effect and parameter choice, but allow for further testing beyond a simple localized derivative term. These strong memory approximations would not require any special consideration beyond standard transport solution techniques. A simple analytical solution is possible using non-Markovian mixed nonscattering materials in a rod model context for comparison.

Key areas of research will be in resolving boundary effects, as well as asymptotic limits for the system. It is hoped that the atomic mix limit, high-contrast mix limit, and diffusion limit will be able to be ascertained over the course of analysis.

References

[1] G. C. Pomraning, *Linear Kinetic Theory and Particle Transport in Stochastic Mixtures*. River Edge, New Jersey, USA: World Scientific Publishing, 1991.

[2] F. Malvagi and R. N. Byrne, "Stochastic radiative transfer in a partially cloudy atmosphere," *Journal of the Atmospheric Sciences*, vol. 50, no. 14, p. 2146, 1992.

[3] A. Abedi and N. Vosoughi, "Neutronic simulation of a pebble bed reactor considering its double heterogeneous nature," *Nuclear Engineering and Design*, vol. 253, p. 277, 2012.

[4] G. C. Pomraning, "Transport in discrete stochastic mixtures," *Transport Theory and Statistical Physics*, vol. 27, p. 405, 1998.

[5] M. L. Adams, E. W. Larsen, and G. C. Pomraning, "Benchmark results for particle transport in a binary markov statistical medium," *Journal of Quantitative Spectroscopy & Radiative Transfer*, vol. 42, p. 253, 1989.

[6] D. S. Miller, F. Graziani, and G. Rodrigue, "Benchmarks and models for time-dependent grey radiation transport with material temperature in binary stochastic media," *Journal of Quantitative Spectroscopy & Radiative Transfer*, vol. 70, p. 115, 2001.

[7] C. Larmier, A. Zoia, F. Malvagi, E. Dumontiel, and A. Mazzolo, "Poisson-box sampling algorithms for three-dimensional markov binary mixtures," *Journal of Quantitative Spectroscopy & Radiative Transfer*, vol. 206, p. 70, 2018.

[8] G. L. Olson, D. S. Miller, E. W. Larsen, and J. E. Morel, "Chord length distributions in binary stochastic media in two and three dimensions," *Journal of Quantitative Spectroscopy & Radiative Transfer*, vol. 101, p. 269, 2006.

[9] A. K. Prinja and G. L. Olson, "Grey radiative transfer in binary stochastic media with material temperature coupling: Asymptotic limits," *Los Alamos National Laboratory*, no. LA-UR-03-1883, 2003.

[10] J. A. Fleck and J. D. Cummings, "An Implicit Monte Carlo scheme for calculating time and frequency dependent nonlinear radiation transport," *Journal of Computational Physics*, vol. 8, p. 313, 1971.

[11] A. Long, "Branson." `https://github.com/lanl/branson`, July 2021.

[12] A. B. Wollaber, "Four decades of Implicit Monte Carlo," *Journal of Computational and Theoretical Transport*, vol. 45, p. 1, 2016.

[13] R. E. Marshak, "Effect of radiation on shock wave behavior," *Physics of Fluids*, vol. 1, 1958.